Significant enhancement of photoresponsivity in As-doped n-$BaSi_2$ epitaxial films by atomic hydrogen passivation

Sho Aonuki[1], Yudai Yamashita[1], Takuma Sato[1,2], Zhihao Xu[1], Kazuhiro Gotoh[3], Kaoru Toko[1], Yoshikazu Terai[4], Noritaka Usami[3] and Takashi Suemasu[1]

[1]*Institute of Applied Physics, University of Tsukuba, Tsukuba, Ibaraki 305-8573, Japan*

[2]*Université Grenoble Alpes, CNRS, CEA, INAC-SyMMES, 38000 Grenoble, France*

[3]*Graduate School of Engineering, Nagoya University, Nagoya 464-8603, Japan*

[4]*Department of Computer Science and Electronics, Kyushu Institute of Technology, Iizuka, Fukuoka 820-8502, Japan*

Corresponding author:

Takashi Suemasu, University of Tsukuba

suemasu@bk.tsukuba.ac.jp

We grew 500 nm-thick lightly arsenic (As)-doped n-$BaSi_2$ epitaxial films at 600 °C by molecular beam epitaxy, and supplied atomic hydrogen (H) in the duration ($t_{BaSi:H}$) of 0–30 min, followed by capping with a 3 nm-thick amorphous Si layer at 180 °C. The photoresponsivity of the $BaSi_2$ films was enhanced by approximately five times by As doping. Deep level transient spectroscopy measurement revealed the disappearance of previously reported two electron traps. The photoresponsivity was further enhanced by approximately six time after the H supply. It reached a maximum at $t_{BaSi:H}$ = 1–10 min, owing to the reduction of defects.

Photovoltaics (PV) systems have been globally deployed and reached a cumulative installed capacity of over 500 GWp in 2018. It is necessary to further deploy PV systems to establish a sustainable energy supply. Crystalline Si solar cells now account for approximately 90% of the market,[1] and its conversion efficiency (η) steadily increased beyond 26% at the research stage.[2] Thin-film solar cell materials such as cadmium telluride, chalcopyrite, and perovskite have also been attracting attention because of their cost effective growth procedure and high η beyond 22%.[3-8] Thin-film Si has also been studied for years by utilizing an efficient light trapping systems.[9-11] Under such circumstances, we have paid special attention to barium disilicide ($BaSi_2$).[12,13] $BaSi_2$ consists of earth-abundant Si and Ba, and has attractive features[12,13] such as a suitable band gap of 1.3 eV, a large optical absorption coefficient (α) of 3×10^4 cm^{-1} at 1.5 eV, and a large minority carrier diffusion length (~ 10 μm), which is larger than the grain size of $BaSi_2$. We have achieved η approaching 10% in p-$BaSi_2$/n-Si heterojunction solar cells[14,15] and recently demonstrated the operation of $BaSi_2$ homojunction solar cells.[16] We are now focusing on the improvement of optical properties of $BaSi_2$ light absorber layers. According to first-principles calculation,[17] Si vacancies (V_{Si}) are most likely to occur among point defects in $BaSi_2$, and generate deep localized states within the band gap, which act recombination centers. Defect characterizations of $BaSi_2$ have been conducted by deep level transient spectroscopy (DLTS),[18,19] positron annihilation spectroscopy,[20,21] Raman spectroscopy,[22] photoluminescence,[23] and electron paramagnetic resonance.[24] By using these techniques, we detected defects, most of which are considered V_{Si}. As a measure to investigate the optical properties of $BaSi_2$ films, we have used photoresponsivity because it is very sensitive to carrier lifetime. Our previous research shows that the photoresponsivity of undoped $BaSi_2$ films is enhanced markedly by supplying atomic hydrogen (H) produced by an radio-frequency (RF) plasma generator after the growth of $BaSi_2$ films for 15 min owing to the increase of carrier lifetime, proved by microwave-detected photoconductivity decay measurement (μ-PCD).[25] This result means that defects in undoped $BaSi_2$ films are passivated by atomic H. As the basic structure of a solar cell is a pn-junction, it is thereby necessary to examine whether or not defects in impurity-doped n-$BaSi_2$ and p-$BaSi_2$ films are passivated by atomic H. Regarding B-doped p-$BaSi_2$ films, the effect of H passivation was very recently demonstrated.[26] On the other hand, there has been no report on the effect of atomic H on As-doped n-$BaSi_2$ films. The valence band maximum of $BaSi_2$ is mainly composed of Si s and p orbitals.[27,28] Therefore, substitution of Si

atoms in $BaSi_2$ with group 15 elements such as As increases the valence electron concentration and forms n-$BaSi_2$.[29] We adopted GaAs granules as a source of As rather than elemental As. It is possible to supply only As from GaAs thanks to a much lower vapor pressure of Ga than that of As.[30] Furthermore, As atoms are supplied in the form of As_2 from GaAs, and are thus more likely to decompose into As atoms than that of As_4 emitted from elemental As.[31]

We fabricated lightly As-doped n-$BaSi_2$ epitaxial films by MBE. An ion-pumped MBE system equipped with an RF plasma generator for atomic H, an electron-beam gun for Si, and Knudsen cells for Ba and GaAs was used. Si(111) substrates were employed for *a*-axis-oriented As-doped n-$BaSi_2$ epitaxial films. The detailed growth method of As-doped $BaSi_2$ epitaxial films has been reported previously.[32] Briefly, after cleaning the Si(111) substrates, we formed a $BaSi_2$ template layer by reactive deposition epitaxy, in which only Ba was supplied to a heated Si substrate. This template layer works as a seed crystal for overlayers. Next, a 500 nm-thick As-doped $BaSi_2$ epitaxial layer was formed by MBE at a substrate temperature (T_S) of 600 °C. We set the temperature of GaAs granules at 300 °C, because the photoresnponsivity of As-doped $BaSi_2$ films reached a maximum at around this temperature.[32] The As concentration (N_{As}) in the As-doped $BaSi_2$ films was below the limit of detection by secondary ion mass spectrometry (SIMS) ($N_{As} < 5 \times 10^{17}$ cm^{-3}). We also fabricated an undoped $BaSi_2$ film for comparison. After that, atomic H was supplied at T_S = 600 °C to As-doped $BaSi_2$ films with various supply durations $t_{BaSi:H}$ of 0, 1, 10, 15, 20, and 30 min. The plasma power was set at 10 W. The flow of atomic H was controlled by a vacuum gauge of the MBE system; the vacuum level was 1.0×10^{-3} Pa during the H supply. Finally, a 3-nm-thick amorphous Si capping layer was formed *in situ* at T_S = 180 °C to prevent surface oxidation. We used Czochralski (CZ)-p-Si(111) substrates (ρ > 1000 Ωcm) for μ-PCD and Raman spectroscopy measurements. On the other hand CZ-n^+-Si(111) substrates (ρ < 0.01 Ωcm) were used for photoresponsivity and DLTS measurements. For this purpose, front surface electrodes with 1-mm-diameter 80 nm-thick ITO and back surface electrodes with 150 nm-thick Al were formed by sputtering. We evaluated the optical properties with a lock-in technique using a xenon lamp (Bunko Keiki, SM-1700A) and a single monochromator with a focal length of 25 cm (Bunko Keiki, RU-60N) under a bias voltage (V_{bias}) of −0.3 or −0.5 V to the surface ITO electrodes with respect to the rear Al electrodes. The intensity of incident light was calibrated with a pyroelectric sensor (Melles Griot, 13PEM001/J). Excess-carrier decay kinetics were evaluated by a μ-PCD measurement system (Kobelco, LTA-

1512EP). Carriers were generated by a 5 ns laser pulse with a wavelength of 349 nm (3.55 eV). The excitation power was 1.3×10^5 Wcm^{-2}. Photoconductivity decay was measured using the reflectivity of a microwave with a frequency of 26 GHz. Polarized Raman spectra were collected to investigate local vibrational modes (LVM) at the $X(YZ)\overline{X}$ geometry of the typical Porto notation using a polarizer. The X-axis was parallel to $BaSi_2$ [100]. In this geometry, the most intense Raman peak of the Ag mode (488 cm^{-1}) can be suppressed since there are only the diagonal constitution of Raman tensor of the Ag mode[33)] so that LVM at around 490 cm^{-1} can be observed. DLTS measurement was performed at 80–300 K. A 1 MHz capacitance-voltage meter (HP 4280A) was used. All measurements except DLTS were carried out at room temperature.

The a-axis-oriented epitaxial growth of all the samples was confirmed by reflection high-energy electron diffraction and θ-2θ X-ray diffraction. The hole concentration of undoped p-$BaSi_2$ films was 8.7×10^{15} cm^{-3} and the electron concentration of As-doped n-$BaSi_2$ films was 7.1×10^{16} cm^{-3}. Figure 1(a) shows the photoresponse spectra of undoped p-$BaSi_2$ and As-doped n-$BaSi_2$ films. The photoresponsivity was obtained at wavelengths smaller than approximately 1000 nm, corresponding to the band gap of $BaSi_2$. The photoresponsivity was apparently improved by As doping. This result is interpreted to originate from the decrease of defects such as V_{Si} because doped As atoms are considered to occupy part of V_{Si} in the films. The photoresponsivity of As-doped $BaSi_2$ films was further improved by atomic H supply and reached a maximum at $t_{BaSi:H}$ =1 and 10 min as shown in Fig. 1(b), wherein the H concentration was of the order of 10^{18}–10^{19} cm^{-3}.[25)] The highest photoresponsivity was approximately six times higher than that of As-doped $BaSi_2$ films without atomic H supply. The photoresponsivity in the short wavelength range (λ = 300–450 nm) was the highest at $t_{BaSi:H}$ = 1 min, and degraded with increasing $t_{BaSi:H}$. Since the α of $BaSi_2$ in such short λ exceeds 5×10^5 cm^{-1},[12)] the penetration depth of the light is estimated to be less than $3/\alpha \sim 60$ nm, meaning that short-λ photons are absorbed in the surface region of $BaSi_2$ films. This result thereby suggests that the surface of $BaSi_2$ films was damaged by atomic H supply. Similar results were obtained for undoped $BaSi_2$ films after the H supply.[25)] At $t_{BaSi:H} \geq 15$ min, however, the photoresponsivity started to degrade. On the other hand, in undoped $BaSi_2$ films, the photoresponsivity reached a maximum at $t_{BaSi:H}$ = 15 min.[25)] It is noted that the photoresponsivity reached a maximum at a shorter value of $t_{BaSi:H}$ (1–10 min) for As-doped $BaSi_2$ films than that for undoped $BaSi_2$ films ($t_{BaSi:H}$ = 15 min). We speculate that the reason for this is that the density of V_{Si} is smaller in As-doped $BaSi_2$ films than

in undoped $BaSi_2$ films, and thus a smaller amount of H atoms are enough to passivate V_{Si} in As-doped $BaSi_2$ films.

According to the significant improvement of the photoresponsivity of the atomic H-passivated $BaSi_2$ films, it is reasonable to consider that the carrier lifetime would be improved for these samples. Figure 2 shows the photoconductivity decay curves. Assuming that the reflectivity of microwaves is proportional to the excess carrier concentration, we can deduce the carrier lifetime from the decay curves. The areal photon density was $(1.3 \times 10^5 \times 5 \times 10^{-9})/(1.6 \times 10^{-19} \times 3.55) \approx 1.1 \times 10^{15}$ cm^{-2}. The photogenerated carrier concentration is thus calculated to be $1.1 \times 10^{15}/(0.5 \times 10^{-4}) = 2.2 \times 10^{19}$ cm^{-3} on average, assuming that photogenerated carriers are uniformly distributed over the 500 nm-thick As-doped $BaSi_2$ films. Hara *et al*. illustrated that the decay curves of $BaSi_2$ films can be fitted by three exponential functions.[34] The first rapid decay curve originates from the Auger recombination, the second decay from the Shockley-Read-Hall (SRH) recombination, and the third one from the SRH recombination accompanying carrier traps. Following this method, we fitted the experimentally obtained curves with dashed lines. Here we define $\tau_{1/e}$ as the time when the reflected microwave intensity decreases by exp(−1) of the initial value after the excitation laser was turned off. As shown in Fig. 2, $\tau_{1/e}$ was determined to be approximately 0.1, 0.8, 2.7, 2.8, and 1.6 μs, respectively, at $t_{BaSi:H}$ = 0, 1, 10, 20, and 30 min. The $\tau_{1/e}$ rapidly increased with $t_{BaSi:H}$ and almost saturated at around $t_{BaSi:H}$ =10–20 min, and then decreased for $t_{BaSi:H} > 20$ min. The general trend seen in Fig. 2, that is, $\tau_{1/e}$ increases with $t_{BaSi:H}$, becomes maximum at a certain value of $t_{BaSi:H}$, and decreases for longer $t_{BaSi:H}$, is the same as that observed for the photoresponsivity against $t_{BaSi:H}$ in Fig. 1(b). However, the optimum $t_{BaSi:H}$ differs between photoresponsivity and $\tau_{1/e}$. We speculate that this disagreement comes from a large difference in a measurement area between the two measurement methods; an area of 1 × 1 cm^2 was used for μ-PCD, while only a 1 mm-diameter area was for photoresponsivity. Therefore, $\tau_{1/e}$ is more likely to be affected by nonuniformity of samples.

To understand the effect of As doping in more detail, we performed the DLTS measurement on As-doped n-$BaSi_2$ films. Regarding the trap levels in undoped $BaSi_2$ films, two electron trap levels positioned at approximately 0.1 and 0.2 eV from the conduction band minimum (CBM) were detected previously.[18,19] Figure 3 (a) shows the DLTS profiles of the As-doped n-$BaSi_2$ film at $t_{BaSi:H}$ =0 min. The forward filling pulse voltage V_P with a pulse width

t_{pw}=50 ms was set at 0.5 V, and the reverse bias voltage V_R was varied as −0.1, −0.5, and −1.0 V. Because of a large difference in electron concentration (n) between n$^+$-Si ($n > 5 \times 10^{18}$ cm^{-3})[35] and As-doped n-$BaSi_2$ ($n \sim 7.1 \times 10^{16}$ cm^{-3}), the depletion region stretches towards the n-$BaSi_2$ side. A downward facing peak due to a majority carrier (electron) trap (E1) was detected at around 200 K. The peak intensity decreased with increasing $|V_R|$, meaning that the traps were positioned around the heterointerface. Figure 3(b) shows the Arrhenius plots of the thermal emission rates (T^2/e_n^t) of captured electrons, where e_n^t is the thermal emission rate and the T is the absolute temperature.[36] The calculated energy levels $E1$ were 0.79, 0.80, and 0.98 eV from the CBM at V_R = −0.1, −0.5, and −1.0 V, respectively. As the As-doped n-$BaSi_2$ films showed higher photoresponsivity than undoped ones, we ascribe such deep levels (0.8–0.9 eV) not to actual defects but to a conduction band offset of approximately 0.8 eV at the $BaSi_2$/Si, caused by a difference in electron affinity between Si(4.05 eV) and $BaSi_2$(3.2 eV).[37] There have been several reports thus far on the detection of band offsets by DLTS for heterointerfaces such as Si/SiGe and GaAs/InGaAs.[38–40] Considering this way, we conclude that the two electron trap levels previously reported decreased significantly by As doping and fell below the limit of detection. As the electron concentration of As-doped n-$BaSi_2$ films is 7.1×10^{16} cm^{-3}, the trap density is considered to be smaller than 10^{15} cm^{-3}. We attribute the defect reduction to doped As atoms occupying part of V_{Si}.

Regarding the experimentally obtained further enhancement of photoresponsivity in As-doped $BaSi_2$ films by H supply, there is a lack of information about the position of atomic H in the lattice of As-doped $BaSi_2$. According to *ab initio* electronic property simulations of $BaSi_2$ with V_{Si} and H incorporation, V_{Si} becomes inactive when two H atoms are in a V_{Si}.[25] Therefore, we speculate that H atoms are also around V_{Si} in As-doped $BaSi_2$ films. Figure 4 shows the Raman shift of the Ag mode deduced from polarized Raman spectra of As-doped $BaSi_2$ films at $t_{BaSi:H}$ = 0–30 min. Typical examples of polarized Raman spectra at $t_{BaSi:H}$ = 0 and 1 min are also shown. One Lorentzian curve at around 488 cm^{-1} is enough to reconstruct the measured spectrum at $t_{BaSi:H}$ = 0 min. However, another Lorentzian curve located at around 493 cm^{-1} is necessary to reconstruct the spectrum at $t_{BaSi:H}$ =1 min. Similar results were obtained for other samples at $t_{BaSi:H} \geq 10$ min. This is the reason why the peak position of the Raman shift was higher than that at $t_{BaSi:H}$ = 0 min. The origin of this new peak is unknown at present; however, there is a

possibility that reflects the bonding of H to a Si atom in Si tetrahedra of the $BaSi_2$ lattice. To identify the origin of this peak, it is necessary to investigate the atomic structure of Si tetrahedral by using first-principles calculation in the near future.

We fabricated As-doped n-$BaSi_2$ films by MBE at T_S = 600 °C and investigated the effect of atomic H supply on their photoresponsivity. The photoresponsivity was enhanced by As doping compared to undoped $BaSi_2$ films. DLTS measurement revealed that the defect density of previously reported two electron traps fell below the detection limit of SIMS. The photoresponsivity was further enhanced by approximately six times when the atomic H was supplied on As-doped $BaSi_2$ films for 1−10 min at T_S = 600 °C. When the atomic H supply duration lengthened further, the photoresponsivity decreased. These results showed the atomic H supply is an effective means to passivate the defects in As-doped n-$BaSi_2$ films and enhance their photoresponsivity.

Acknowledgements

This work was financially supported by JSPS KAKENHI Grant Numbers 18H01477 and 18H03767. One of the authors (Y. Y.) was financially supported by Grant-in-Aid for JSPS Fellows (19J21372).

Captions of figures

Fig. 1 Photoresponse spectra of (a) undoped and As-doped $BaSi_2$ films at V_{bias} = –0.5 V, and (b) As-doped $BaSi_2$ films grown with different values of $t_{BaSi:H}$ = 0 – 30 min at V_{bias} = –0.3 V. All the samples were grown at T_S = 600 °C for As doping.

Fig. 2 Photoconductivity decay curves of As-doped $BaSi_2$ films grown with different values of $t_{BaSi:H}$ = 0 – 30 min. The fitting lines are shown as dashed lines.

Fig. 3 (a) DLTS profiles obtained for n-$BaSi_2$/n-Si diodes on the CZ n^+-Si(111) substrate. The forward filling pulse voltage V_P was set at 0.5 V with a pulse width of t_{pw} = 50 ms, and the reverse-bias voltage V_R was set at −0.1, −0.5, and −1.0 V. The rate window was varied as 1–32, 2–64, 4–128, 8–256, and 16–512 ms. (b) Arrhenius plots of the thermal emission rates (T^2/e_n^t) for electron trap level ($E1$) observed for As-doped n-$BaSi_2$ films at V_R = −0.1, −0.5, and −1.0 V. Here, e_n^t is the thermal emission rate and T is the absolute temperature.

Fig. 4 Raman shift of the Ag mode as a function of $t_{BaSi:H}$ for As-doped $BaSi_2$ films obtained for polarized Raman spectra at the $X(YZ)\overline{X}$ geometry. Typical examples of the spectra for samples grown with $t_{BaSi:H}$ = 0 and 1 min are shown. The fitting lines are shown as dashed lines.

References

1) M. A. Green, E. D. Dunlop, D. H. Levi, J. Hohl-Ebinger, M. Yoshita, and A. W. Y. Ho-Baillie, Prog. Photovoltaics Res. Appl. **27**, 565 (2019).

2) K. Yoshikawa, H. Kawasaki, W. Yoshida, K. Konishi, K. Nakano, T. Uto, D. Adachi, M. Kakematsu, H. Uzu, and K. Yamamoto, Nat. Energy **2**, 17032 (2017).

3) J. Britt and C. Ferekides, Appl. Phys. Lett. **62**, 2851 (1993).

4) A. Romeo, A. Terheggen, D. Abou-Ras, D. L. Batzner, F. J. Haug, M. Kalin, D. Rudmann, and A. N. Tiwari, Prog. Photovoltaics **12**, 93 (2004).

5) X. Wu, Sol. Energy **77**, 803 (2004).

6) I. Repins, M. A. Contreras, B. Egaas, C. DeHart, J. Scharf, C. L. Perkins, B. To, and R. Noufi, Prog. Photovoltaics **16**, 235 (2008).

7) H. Katagiri, K. Jimbo, W. S. Maw, K. Oishi, M. Yamazaki, H. Araki, and A. Takeuchi, Thin Solid Films **517**, 2455 (2009).

8) P. Jackson, R. Wuerz, D. Hariskos, E. Lotter, W. Witte, and M. Powalla, Phys. Status Solidi Rapid Research Lett. **10**, 583 (2016).

9) D. Zhou and R. Biswas, J. Appl. Phys. **103**, 093102 (2008).

10) A. Hongsingthong, T. Krajangsang, I. A. Yunaz, S. Miyajima, and M. Konagai, Appl. Phys. Express **3**, 051102 (2010).

11) H. Sai, Y. Kanamori, and M. Kondo, Appl. Phys. Lett. **98**, 113502 (2011).

12) T. Suemasu, Jpn. J. Appl. Phys. **54**, 07JA01 (2015).

13) T. Suemasu and N. Usami, J. Phys. D. Appl. Phys. **50**, 023001 (2017).

14) S. Yachi, R. Takabe, H. Takeuchi, K. Toko, and T. Suemasu, Appl. Phys. Lett. **109**, 072103 (2016).

15) T. Deng, T. Sato, Z. Xu, R. Takabe, S. Yachi, Y. Yamashita, K. Toko, and T. Suemasu, Appl. Phys. Express **11**, 062301 (2018).

16) K. Kodama, Y. Yamashita, K. Toko, and T. Suemasu, Appl. Phys. Express **12**, 041005 (2019).

17) M. Kumar, N. Umezawa, W. Zhou, and M. Imai, J. Mater. Chem. A **5**, 25293 (2017).

18) H. Takeuchi, W. Du, M. Baba, R. Takabe, K. Toko, and T. Suemasu, Jpn. J. Appl. Phys. **54**, 07JE01 (2015).

19) Y. Yamashita, T. Sato, N. Saitoh, N. Yoshizawa, K. Toko, and T. Suemasu, J. Appl. Phys. **126**, 215301 (2019).
20) Y. Yamashita, Y. Takahara, T. Sato, K. Toko, A. Uedono, and T. Suemasu, Appl. Phys. Express **12**, 055506 (2019).
21) A. Montes, S. W. Eijt, Y. Tian, R. Gram, H. Schut, T. Suemasu, N. Usami, M. Zeman, J. Serra, and O. Isabella, J. Appl. Phys. **127**, 085304 (2020).
22) T. Sato, H. Hoshida, R. Takabe, K. Toko, Y. Terai, and T. Suemasu, J. Appl. Phys. **124**, 025301 (2018).
23) T. Sato, Y. Yamashita, Z. Xu, K. Toko, S. Gambarelli, M. Imai, and T. Suemasu, Appl. Phys. Express **12**, 111001 (2019).
24) T. Sato, C. Lombard, Y. Yamashita, Z. Xu, L. Benincasa, K. Toko, S. Gambarelli, and T. Suemasu, Appl. Phys. Express **12**, 061005 (2019).
25) Z. Xu, D. A. Shohonov, A. B. Filonov, K. Gotoh, T. Deng, S. Honda, K. Toko, N. Usami, D. B. Migas, V. E. Borisenko, and T. Suemasu, Phys. Rev. Mater. **3**, 065403 (2019).
26) L. Benincasa, Z. Xu, T. Deng, T. Sato, K. Toko, and T. Suemasu, Jpn. J. Appl. Phys. **59**, SFFA08 (2020).
27) Y. Imai and A. Watanabe, Intermetallics **15**, 1291 (2007).
28) D. B. Migas, V. L. Shaposhnikov, and V. E. Borisenko, Phys. Status Solidi B **244**, 2611 (2007).
29) K. O. Hara, N. Usami, M. Baba, K. Toko, and T. Suemasu, Thin Solid Films **567**, 105 (2014).
30) J. R. Arthur, J. Phys. Chem. Solids **28**, 2257 (1967).
31) C. T. Foxon, J. A. Harvey, and B. A. Joyce, J. Phys. Chem. Solids **34**, 1693 (1973).
32) S. Aonuki, Y. Yamashita, K. Toko, and T. Suemasu, Jpn. J. Appl. Phys. **59**, SFFA01 (2020).
33) H. Hoshida, N. Murakoso, T. Suemasu, and Y. Terai, Defect Diffus. Forum **386**, 43 (2018).
34) K. O. Hara, N. Usami, K. Toh, M. Baba, K. Toko, and T. Suemasu, J. Appl. Phys. **112**, 083108 (2012).
35) S. M. Sze, Physics of Semiconductor Devices (Wiley, New York, 1981) 2nd ed.
36) D. V. Lang, J. Appl. Phys. **45**, 3023 (1974).
37) T. Suemasu, K. Morita, M. Kobayashi, M. Saida, and M. Sasaki, Jpn. J. Appl. Phys. **45**, L519 (2006).
38) L. Vescan, R. Apetz, and H. Lüth, J. Appl. Phys. **73**, 7427 (1993).

39) L. Lu, J. Wang, Y. Wang, W. Ge, G. Yang, and Z. Wang, J. Appl. Phys. **83**, 2093 (1998).

40) L. Lu, S. Su, C. C. Ling, S. Xu, D. Zhao, J. Zhu, H. Yang, J. Wang, and W. Ge, Appl. Phys. Express **5**, 091001 (2012).

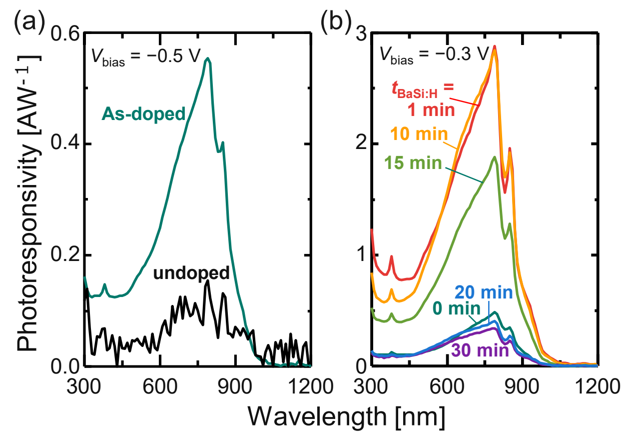

Fig. 1

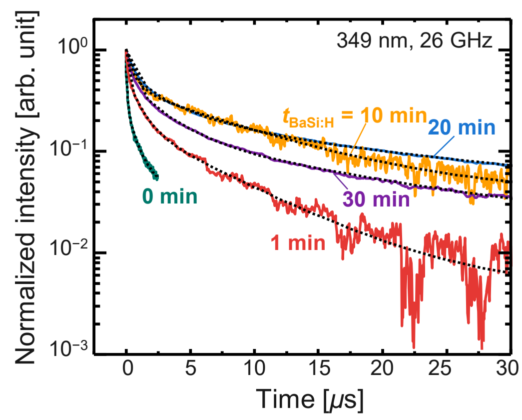

Fig. 2

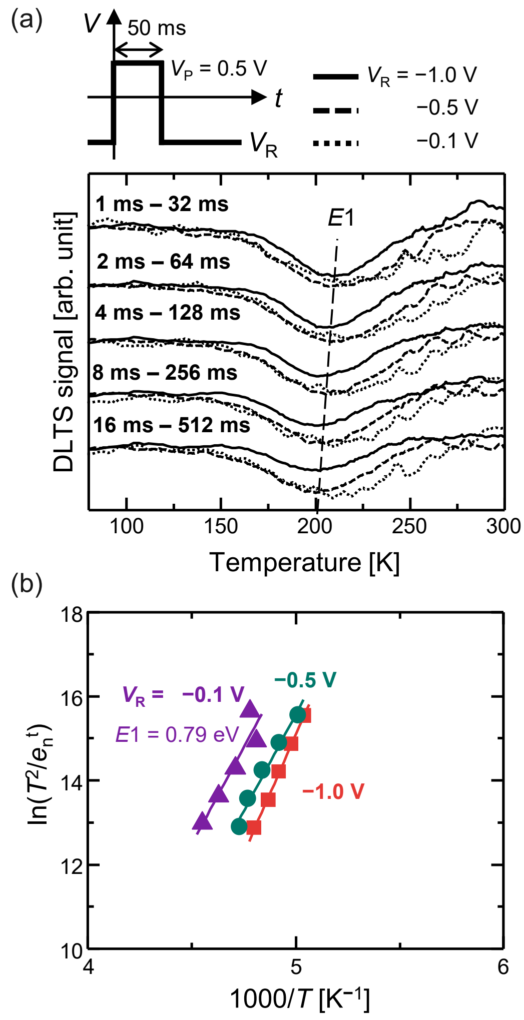

Fig. 3

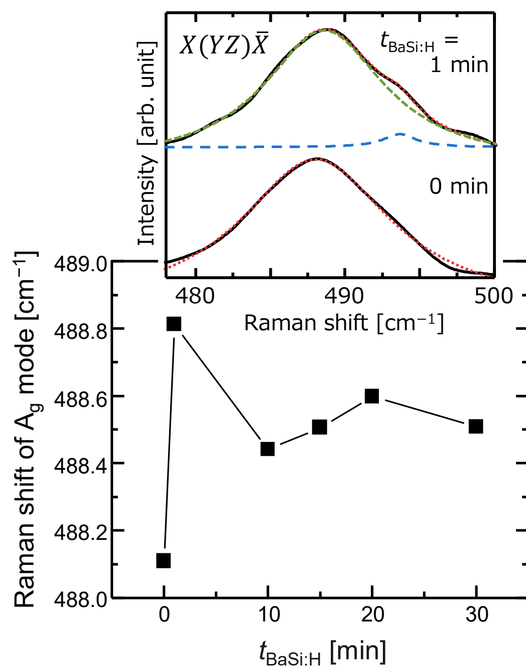

Fig. 4